Electronic Supplementary Material (ESI) for Nanoscale.

Investigation of Local Distortion Effects on X-Ray Absorption of Ferroelectric Perovskites from First Principles Simulations

*Pedram Abbasi, David P. Fenning, Tod A. Pascal**

Department of Nano and Chemical Engineering, University of California San Diego, La Jolla, CA 92093, USA

***Corresponding author:** tpascal@ucsd.edu

Supplementary Information:

Table of Contents

Experimental XAS Measurements:

Experimental XAS result were obtained on a BaTiO3 thin films (~10 nm thick) synthesized by reactive MBE deposited on (0.5 wt.%) Nb-doped (001)-oriented $SrTiO_3$ substrates. The detail of growth is discussed in detail in our previous work.[1] XAS experiments were performed at the XTIP[2] beamline 4-ID-E of the Advanced Photon Source and Center for Nanoscale Materials in Argonne National Laboratory. Polarization reversal was achieved by biasing sample with ±10V with an STM tip in tunneling mode for 10 minutes. O-K and Ti-L edges were probed by XAS spectra was achieved by changing the beam energy from 525 to 545eV and 453.5 to 468.5eV with a step size of 0.1eV to probe, respectively.

First-Principles Computational XAS:

First-principles XAS simulations were perform on a 1x1x5 symmetric slab with ~15A of vacuum at each side. To model the $BaTiO_3$ thin film, we used a tetragonal (*P4mm*) unit cell with a lattice constant of a=3.99 Å and c=4.03 Å. Implementing periodic boundary conditions (PBC) on the slab geometry is critical to mimic the properties of an experimental thin film with broken symmetry along the z axis, while enabling the possibility of creating surface sites and local distortion effects. Moreover, limiting the supercell size to 1x1x5, with less than 30 atoms, makes tractable the computationally demanding, non-self-consistent electronic and BSE screening calculations. To represent the upward and downward polarization states and symmetry breaking across the slab model, the topmost layer was distorted as detailed in Table 1. The calculated local polarization (per unit cell), based on a berry-phase[3] model for each of these distortions, is also listed.

Here upward distortion of Ti atoms within the oxygen octahedron toward the surface of slab model (vacuum) is denoted as P^+, while a downward displacement toward the film is denoted as P^-.

(i) Many-body ΔSCF determinant approach:

The results based on the many-body ΔSCF determinant formalism was simulated using MBXAS code.[4] Ground state DFT calculations were performed with Quantum ESPRESSO.[5] The generalized gradient approximation of Perdew, Burke, and Ernzerhof (PBE)[6] was used to properly describe O-p and Ti-d orbitals of $BaTiO_3$. Supercell calculations were performed with 2 × 2 × 2 k-point grids. The calculations used a 30 Ry kinetic energy and 300 Ry charge-density cutoff, with a gaussian broadening of 0.2 eV. The core-excited electronic structure and associated orbitals used in spectral line-shape calculations were computed within the full-core hole (FCH) approximation. The spectra for different materials and for different excited sites within the same material were aligned based on the position of the main edge of the element in the experimental dataset. The 1s core-excited O atom was simulated using a pseudo-potential with configuration of $1s^1\ 2s^2\ 2p^4$.

In many-body determinant ΔSCF approach is the equilibrated electron density in the presence of a core hole, while the initial state is taken as the ground state of the pristine system.[4] The transition amplitude is approximated based on using the Kohn-Sham orbitals, based on the following equation:

$$\langle \psi_f | \varepsilon \,.\, R | \psi_i \rangle = S \langle \psi_f | \varepsilon \,.\, r | \psi_h \rangle$$

where ε stand for photon polarization, R is the many-body position operator, ψ_f is the unoccupied orbitals in the final state, and $\psi_h$is the core orbital in the initial state. S is a many-body overlap that reflects the excited-state response of the remaining electrons other than the photoexcited one.[4]

(ii) Hybrid GW/BSE Approach:

Computational XAS results were obtained based on BSE approach using OCEAN 2.9.7 (Obtaining Core Excitations from Ab initio electronic structure and NBSE) code.[7] Ground state DFT calculations were obtained using Quantum ESPRESSO,[5] with norm-conserving pseudopotentials from the pseudo-dojo distribution. A 2 x 2 x 2 k-point grid was used to solve the Kohn–Sham equations, and a total of ~1700 bands were used for the screening calculations. The final state is assumed to be a superposition of effective e-h pairs, whose matrix elements are calculated based on the following equation:

$$\langle \psi_f | \varepsilon \,.\, R | \psi_i \rangle = \sum_c A^{f}{}_{c}^{*} \, \langle \psi_c | \varepsilon \,.\, r | \psi_h \rangle$$

where ψ_c are the initial-state orbitals and c iterates over empty orbitals only. The exciton amplitude $A^{f}{}_{c}^{*}$ and energy Ef can be solved from the BSE method.[4]

Supplementary Tables:

Table S1. Values for local distortions associated with different extent of upward and downward polarization, noted as P1 and P2.

Polarization	Relative Distortion (*d/c*)	Absolute Distortion (Å)	Berry Phase Polarization
P1	0.0215	0.087	18 μC/cm^2
P2	0.0430	0.174	32 μC/cm^2

Table S2. Values for relative peak ratios on O-K edge of the surfaces in upward and downward polarization based on experimental data and calculations with P1 and P2 polarization values.

***O-K* Experiment**				
Peak	**P+/P-**		**P+**	**P-**
t_{2g}	1.17	t_{2g} / e_g	1.31	1.29
e_g	1.14			
O-K ΔSCF (P1)				
t_{2g}	1.05	t_{2g} / e_g	1.03	1.14
e_g	1.16			
O-K ΔSCF (P2)				
t_{2g}	1.09	t_{2g} / e_g	0.94	1.07
e_g	1.25			
O-K BSE (P1)				
t_{2g}	1.09	t_{2g} / e_g	1.90	1.73
e_g	0.99			
O-K BSE (P2)				
t_{2g}	1.22	t_{2g} / e_g	2.19	1.49
e_g	0.83			

Table S3. Values for relative peak ratios on O-K edge of the surfaces in upward and downward polarization based on experimental data and calculations with P1 and P2 polarization values.

***Ti-L* Experiment**				
Peak	**P+/P-**		**P+**	**P-**
L3- t_{2g}	1.18	**L3 t_{2g} / e_g**	0.64	0.64
L3- e_g	1.17			
L2- t_{2g}	1.30	**L2 t_{2g} / e_g**	0.56	0.52
L2- e_g	1.21			
Ti-L ΔSCF (P1)				
L3- t_{2g}	1.12	**L3 t_{2g} / e_g**	1.93	1.86
L3- e_g	1.07			
L2- t_{2g}	N/A	**L2 t_{2g} / e_g**	N/A	N/A
L2- e_g	N/A			
Ti-L ΔSCF (P2)				
L3- t_{2g}	1.15	**L3 t_{2g} / e_g**	1.88	1.86
L3- e_g	1.14			
L2- t_{2g}	N/A	**L2 t_{2g} / e_g**	N/A	N/A
L2- e_g	N/A			
Ti-L BSE (P1)				
L3- t_{2g}	1.03	**L3 t_{2g} / e_g**	0.49	0.55
L3- e_g	1.11			
L2- t_{2g}	1.05	**L2 t_{2g} / e_g**	0.66	0.80
L2- e_g	1.09			
Ti-L BSE (P2)				
L3- t_{2g}	1.17	**L3 t_{2g} / e_g**	0.66	0.80
L3- e_g	1.13			
L2- t_{2g}	1.23	**L2 t_{2g} / e_g**	0.59	0.70
L2- e_g	1.09			

Supplementary Figures:

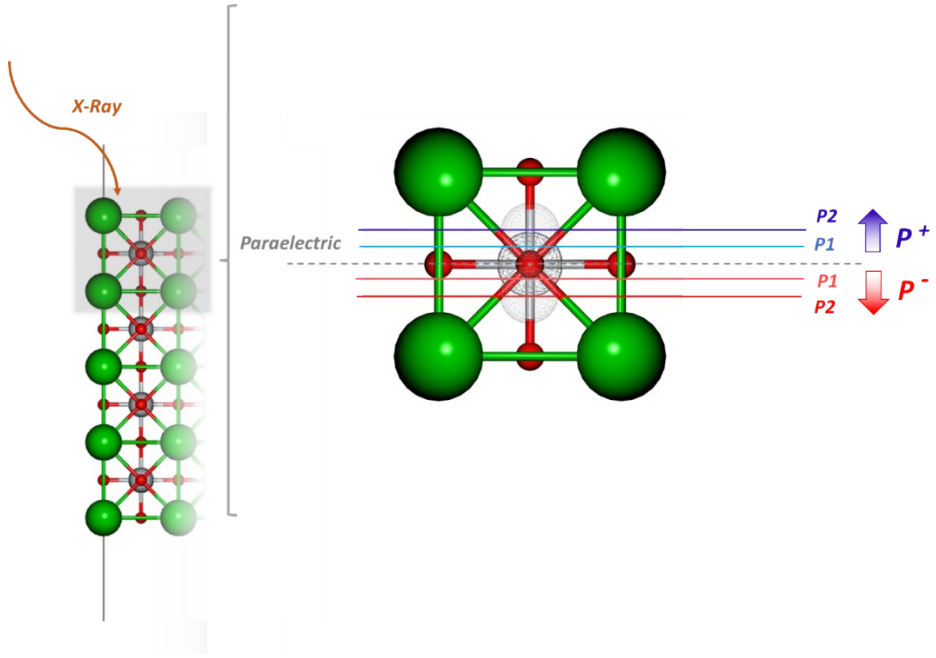

Figure S1. Schematic of the slabs used for XAS calculations, slab with different extent of upward and downward polarization, noted as P1 and P2.

Supplementary References:

(1) Abbasi, P.; Barone, M. R.; de la Paz Cruz-Jáuregui, M.; Valdespino-Padilla, D.; Paik, H.; Kim, T.; Kornblum, L.; Schlom, D. G.; Pascal, T. A.; Fenning, D. P. Ferroelectric Modulation of Surface Electronic States in BaTiO 3 for Enhanced Hydrogen Evolution Activity. *Nano Lett.* **2022**, *22* (10), 4276–4284. https://doi.org/10.1021/acs.nanolett.2c00047.

(2) Rose, V.; Shirato, N.; Bartlein, M.; Deriy, A.; Ajayi, T.; Rosenmann, D.; Hl, S. W.; Fisher, M.; Reininger, R. XTIP - The World's First Beamline Dedicated to the Synchrotron X-Ray Scanning Tunneling Microscopy Technique. *J. Synchrotron Radiat.* **2020**, *27*, 836–843. https://doi.org/10.1107/S1600577520003689.

(3) Berry, M. V. Quantal Phase Factors Accompanying Adiabatic Changes. *A Half-century Phys. Asymptotics Other Divers. Sel. Work. By Michael Berry* **2017**, *392* (1802), 72–84. https://doi.org/10.1142/9789813221215_0006.

(4) Liang, Y.; Vinson, J.; Pemmaraju, S.; Drisdell, W. S.; Shirley, E. L.; Prendergast, D. Accurate X-Ray Spectral Predictions: An Advanced Self-Consistent-Field Approach Inspired by Many-Body Perturbation Theory. *Phys. Rev. Lett.* **2017**, *118* (9). https://doi.org/10.1103/PhysRevLett.118.096402.

(5) Giannozzi, P.; Baroni, S.; Bonini, N.; Calandra, M.; Car, R.; Cavazzoni, C.; Ceresoli, D.; Chiarotti, G. L.; Cococcioni, M.; Dabo, I.; Dal Corso, A.; De Gironcoli, S.; Fabris, S.; Fratesi, G.; Gebauer, R.; Gerstmann, U.; Gougoussis, C.; Kokalj, A.; Lazzeri, M.; Martin-Samos, L.; Marzari, N.; Mauri, F.; Mazzarello, R.; Paolini, S.; Pasquarello, A.; Paulatto, L.; Sbraccia, C.; Scandolo, S.; Sclauzero, G.; Seitsonen, A. P.; Smogunov, A.; Umari, P.;

Wentzcovitch, R. M. QUANTUM ESPRESSO: A Modular and Open-Source Software Project for Quantum Simulations of Materials. *J. Phys. Condens. Matter* **2009**. https://doi.org/10.1088/0953-8984/21/39/395502.

(6) Perdew, J. P.; Burke, K.; Wang, Y. Generalized Gradient Approximation for the Exchange-Correlation Hole of a Many-Electron System. *Phys. Rev. B* **1996**, *54* (23), 16533–16539. https://doi.org/10.1103/PhysRevB.54.16533.

(7) Vinson, J.; Rehr, J. J.; Kas, J. J.; Shirley, E. L. Bethe-Salpeter Equation Calculations of Core Excitation Spectra. *Phys. Rev. B - Condens. Matter Mater. Phys.* **2011**. https://doi.org/10.1103/PhysRevB.83.115106.